



# How Molecular Chiralities of Bis(mandelato)borate Anions Affect Their Binding Structures With Alkali Metal Ions and Microstructural Properties in Tetraalkylphosphonium Ionic Liquids

Han-Wen Pei<sup>1</sup>, Bin Li<sup>2</sup>, Aatto Laaksonen<sup>1,3,4</sup> and Yong-Lei Wang<sup>1\*</sup>

<sup>1</sup> Arrhenius Laboratory, Department of Materials and Environmental Chemistry, Stockholm University, Stockholm, Sweden,

<sup>2</sup> School of Chemical Engineering and Technology, Sun Yat-sen University, Zhuhai, China, <sup>3</sup> State Key Laboratory of Materials-Oriented and Chemical Engineering, Nanjing Tech University, Nanjing, China, <sup>4</sup> Centre of Advanced Research in Bionanoconjugates and Biopolymers, Petru Poni Institute of Macromolecular Chemistry, Iasi, Romania

## OPEN ACCESS

### Edited by:

Faiz Ullah Shah,  
Luleå University of Technology,  
Sweden

### Reviewed by:

Jens Smiatek,  
University of Stuttgart, Germany  
Ramesh L. Gardas,  
Indian Institute of Technology Madras,  
India

### \*Correspondence:

Yong-Lei Wang  
wangyoni@gmail.com;  
yonglei.wang@mmk.su.se

### Specialty section:

This article was submitted to  
Physical Chemistry and Chemical  
Physics,  
a section of the journal  
Frontiers in Chemistry

**Received:** 22 October 2019

**Accepted:** 20 January 2020

**Published:** 12 February 2020

### Citation:

Pei H-W, Li B, Laaksonen A and  
Wang Y-L (2020) How Molecular  
Chiralities of Bis(mandelato)borate  
Anions Affect Their Binding Structures  
With Alkali Metal Ions and  
Microstructural Properties in  
Tetraalkylphosphonium Ionic Liquids.  
*Front. Chem.* 8:65.  
doi: 10.3389/fchem.2020.00065

Spiroborate anion-based inorganic electrolytes and ionic liquids (ILs) have fascinating electrochemical and tribological properties and have received widespread attention in industrial applications. The molecular chiralities of spiroborate anions have a significant effect on the microstructures and macroscopic functionalities of these ionic materials in application and thus deserve fundamental consideration. In the current work, we performed quantum chemistry calculations to address the binding strength and coordination structures of chiral bis(mandelato)borate ([BMB]) anions with representative alkali metal ions, as well as the electronic properties of alkali metal ion-[BMB] ion pair complexes. The optimized [BMB] conformers are categorized into V-shaped, bent, and twisted structures with varied electrostatic potential contours and conformational energies and distinct alkali metal ion-[BMB] binding structures. Alkali metal ions have additional associations with phenyl groups in V-shaped [BMB] conformers owing to preferential cation- $\pi$  interactions. Furthermore, the effects of the molecular chiralities of [BMB] anions on the thermodynamics and microstructural properties of tetraalkylphosphonium [BMB] ILs were studied by performing extensive atomistic interactions. Oxygen atoms in [BMB] anions have competitive hydrogen bonding interactions with hydrogen atoms in cations depending on the molecular chiralities and steric hindrance effects of [BMB] anions. However, the molecular chiralities of [BMB] anions have a negligible effect on the liquid densities of tetraalkylphosphonium [BMB] ILs and the spatial distributions of boron atoms in anions around phosphorous atoms in cations. Enlarging tetraalkylphosphonium cation sizes leads to enhanced cation-anion intermolecular hydrogen bonding and Coulombic interactions due to enhanced segregation of polar groups in apolar networks in heterogeneous IL matrices, as verified by scattering structural functions.

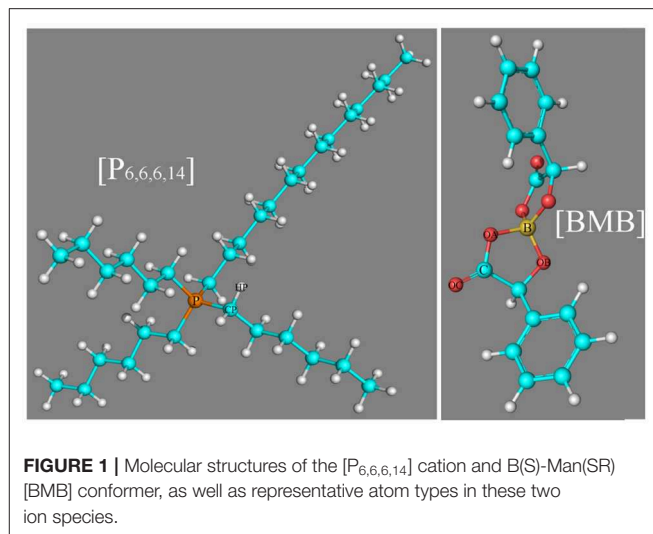
**Keywords:** molecular chiralities, bis(mandelato)borate anions, DFT calculations and atomistic simulations, tetraalkylphosphonium ionic liquids, alkali metal ions

## 1. INTRODUCTION

Ionic liquids (ILs) represent an intriguing category of molten salts solely composed of inorganic or organic anions and, most commonly, organic cations with melting points at or close to room temperature (Castner et al., 2011; Hayes et al., 2015; Zhang et al., 2016; Bedrov et al., 2019). In recent years, ILs have received significant attention in diverse academic and industrial communities due to their multifaceted physicochemical properties, such as non-flammability, negligible volatility, reasonable viscosity-temperature features, high thermal-oxidative stabilities, wide electrochemical windows, and outstanding affinities to polar and apolar compounds (Armand et al., 2009; Zhou et al., 2009; Castner et al., 2011; Wang et al., 2012; Hayes et al., 2015; Dai et al., 2017; Bedrov et al., 2019). These fascinating characteristics can be widely tuned in a controllable fashion via a judicious selection of ion moieties and by mutating specific atoms in constituent ion species (Kashyap et al., 2013; Wang et al., 2014, 2017b; Jankowski et al., 2016; Wu et al., 2016), making ILs exceptionally attractive and reliable alternatives to conventional molecular liquids in applications spanning from solvents in materials synthesis to electrolytes in electrochemical devices (Armand et al., 2009; Zhou et al., 2009; Castner et al., 2011; Abbott et al., 2013; Zhang et al., 2016; Dai et al., 2017; Watanabe et al., 2017; Bedrov et al., 2019).

ILs consisting of spiroborate anions coupled with tetraalkylphosphonium, pyrrolidinium, and imidazolium cations present practical tribological advantages and can be used as alternative high-performance lubricants and lubricant additives in tribology due to their outstanding friction-reducing and anti-wear performance in comparison with conventional fully formulated engine oil in tribological contact with a wide variety of solid materials (Shah et al., 2011, 2013, 2018; Taher et al., 2014; Gusain et al., 2017; An et al., 2018; Pilkington et al., 2018; Hjalmarsson et al., 2019; Rohlmann et al., 2019). Therefore, the number of fundamental studies and industrial applications of spiroborate anion-based ILs has been growing rapidly in recent years.

Besides variations in cation structures, the molecular chiralities of spiroborate anions have a significant effect on the microstructures and dynamics, mesoscopic liquid morphologies, and macroscopic functionalities of these ILs in tribology, electrochemistry, and pharmaceutical chemistry (Yu et al., 2008; Absalan et al., 2012; Sedghamiz and Bahrami, 2019). The bis(mandelato)borate ([BMB]) anion-based ILs are used as selectors for chiral discrimination of propranolol enantiomers (Sedghamiz et al., 2018; Sedghamiz and Bahrami, 2019). Both experimental (Absalan et al., 2012) and computational studies (Sedghamiz et al., 2018; Sedghamiz and Bahrami, 2019) showed that [BMB] anions contribute to distinct hydrogen bonding (HB) and  $\pi$ - $\pi$  stacking interactions with propranolol enantiomers, leading to the formation of propranolol-[BMB] complexes with varied molecular stabilities depending on the specific chiralities of [BMB] anions. In another work, Wong and coworkers presented experimental evidence that [BMB] anions are effective resolving agents for the resolution of a chemically diverse range of racemic



cations via metathesis crystallization (Wong et al., 2015, 2017, 2018).

The significance of [BMB] anions with different molecular chiralities being sensitive to local ionic environments motivates us to explore their delicate associations with alkali metal ions and tetraalkylphosphonium cations, which may provide valuable information for the selection and design of suitable electrolytes and lubricant additives with desirable physicochemical, structural, and functional properties for applications in electrochemistry and tribology (Shah et al., 2011, 2013, 2018; Jankowski et al., 2016; An et al., 2018; Pilkington et al., 2018; Franco et al., 2019; Hjalmarsson et al., 2019). In the current work, we performed intensive density functional theory (DFT) calculations to study the effects of the molecular chiralities of [BMB] anions on their specific binding structures with representative alkali metal ions and, thereafter, extensive atomistic simulations to explore the delicate interactions of [BMB] anions with tetraalkylphosphonium cations with varied alkyl substituents. Three tetraalkylphosphonium cations, namely tetrabutylphosphonium ( $[P_{4,4,4,4}]$ ), tributylhexylphosphonium ( $[P_{4,4,4,8}]$ ), and trihexyltetradecylphosphonium ( $[P_{6,6,6,14}]$ ), and six [BMB] conformers with different molecular chiralities are considered in present work. A schematic molecular structure of the  $[P_{6,6,6,14}]$  cation and B(S)-Man(SR) [BMB] conformer, as well as representative atom types in these two ions are present in **Figure 1**.

## 2. BINDING STRUCTURES OF [BMB] ANIONS WITH ALKALI METAL IONS

DFT calculations were first performed to optimize the molecular geometries of single [BMB] conformers and, thereafter, their tight binding ion-pair structures with alkali metal ions, respectively, using Gaussian 09 package (Frisch et al., 2009) (version D.01) at the B3LYP/6-311+G(d) level of theory (Lee et al., 1988) with Grimme's-D3 dispersion correction (Grimme et al., 2010). This dispersion correction is appropriate over medium ( $\approx 2$ – $5$  Å) and

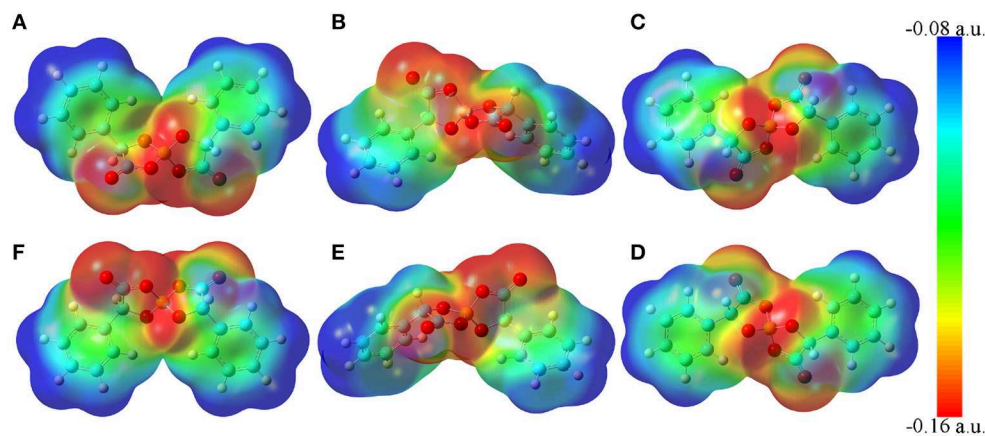


**FIGURE 2** | Molecular electrostatic potential contours of six [BMB] conformers with different molecular chiralities obtained from DFT calculations. **(A)** B(R)-Man(RR), **(B)** B(R)-Man(RS), **(C)** B(R)-Man(SS), **(D)** B(S)-Man(RR), **(E)** B(S)-Man(SR), and **(F)** B(S)-Man(SS).

long ranges ( $> 5 \text{ \AA}$ ) and is an effective method for obtaining the binding structures of complexes with reduced computational cost. Only molecular geometries with all positive vibrational frequencies were taken into consideration to ensure that the obtained anion structures of [BMB] conformers are in fact true minima in the corresponding energy landscapes.

The molecular electrostatic potential contours of six [BMB] conformers based on their respective optimized ion structures are present in **Figure 2**. These optimized [BMB] conformers have remarkable molecular shapes and can be categorized into three pairs, that is, the B(R)-Man(RR) and B(S)-Man(SS) [BMB] conformers (**Figures 2A,F**) are characterized by V-shaped structures, the B(R)-Man(RS) and B(S)-Man(SR) [BMB] conformers (**Figures 2B,E**) have bent conformations, and the B(R)-Man(SS) and B(S)-Man(RR) [BMB] conformers (**Figures 2C,D**) have twisted configurations. Each pair has symmetric ion structures and electrostatic potential contours and is characterized by similar relative conformational energies, dipole moments, and molecular volumes. These computational data are listed in **Table 1**. Previous DFT calculations indicated that boron-based chiral anions are energetically similar in diastereomeric [BMB] systems (Wong et al., 2018). In the current work, the B(R)-Man(RS) and B(S)-Man(SR) [BMB] conformers have the lowest conformational energies, whereas the B(R)-Man(SS) and B(S)-Man(RR) [BMB] conformers have the highest conformational energies, attributing to unbalanced intramolecular forces within [BMB] anionic frameworks. It is noted that the conformational energy difference between all these [BMB] conformers is less than 1 kJ/mol, indicating that these [BMB] conformers may co-exist in IL samples, which is consistent with the results obtained from NMR spectra (Wong et al., 2015). However, the precipitation of twisted B(R)-Man(SS) and B(S)-Man(RR) [BMB] conformers rather than the V-shaped B(R)-Man(RR) and B(S)-Man(SS) [BMB] conformers is always observed in crystallized salts (Wong et al., 2015, 2017). DFT calculations showed that, in all [BMB] conformers, four oxygen atoms exhibit tetrahedral-like distributions around central boron

**TABLE 1** | Relative conformational energies (RCEs) (in kJ/mol), dipole moments (DMs) (in Debye), and molecular volumes (in  $\text{cm}^3/\text{mol}$ ) of single [BMB] conformers, and relative binding energies (RBEs) (in kJ/mol) of varied [BMB] conformers in coordinating alkali metal ions ( $\text{Li}^+$ ,  $\text{Na}^+$ , and  $\text{K}^+$ ), as determined from DFT calculations.

Conformers	Single [BMB] conformers			Alkali metal ion-[BMB] ion pairs		
	RCEs	DMs	Volumes	Li-BMB	Na-BMB	K-BMB
B(R)-Man(RR)	0.0982	6.8945	191.770	-3.0179	-7.5136	-9.5608
B(R)-Man(RS)	0.0000	4.9898	225.871	-0.3833	-1.1197	-4.2263
B(R)-Man(SS)	0.4638	1.6472	248.534	-0.1394	-0.8400	0.0000
B(S)-Man(RR)	0.4642	1.6474	249.508	0.0000	0.0000	-0.3294
B(S)-Man(SR)	0.0020	4.9898	226.122	-1.9355	-0.9143	-4.6534
B(S)-Man(SS)	0.0986	6.8947	192.447	-3.0175	-7.5135	-8.9812

atoms, whereas two oxalato rings have constrained distributions. The addition of phenyl groups to central oxalato moieties results in distorted orientations of phenyl groups around oxalato rings. These distinct conformational variations of [BMB] anions lead to their varied dipole moments and molecular volumes, as listed in **Table 1**. The central moieties in [BMB] anions are polar and have a significant negative charge, leading to varied HB capabilities of three oxygen atom types with HP atoms (as labeled in **Figure 1**) in tetraalkylphosphonium cations (Wang et al., 2015a) and with polar solute molecules, like water (Wang et al., 2015a, 2016).

In addition, the optimized binding structures of varied [BMB] conformers with representative alkali metal ions ( $\text{Li}^+$ ,  $\text{Na}^+$ , and  $\text{K}^+$ ) were determined from intensive DFT calculations at the same level of theory as that used for the calculation of single [BMB] conformers. Furthermore, the binding energies (in kJ/mol) of varied [BMB] conformers with alkali metal ions were determined as the energy difference between the optimized alkali metal ion-[BMB] complexes and the summation of the conformational energies of separately optimized ion species. These binding energies are corrected for basis sets superposition error (BSSE) using the counterpoise procedure (Boys and

Bernardi, 1970). The relative binding energies of three alkali metal ions with six [BMB] conformers are listed in **Table 1**, and the corresponding optimized ion-pair structures are shown in **Figures 3–5**, respectively.

All these alkali metal ions exhibit specific associations with central polar moieties of [BMB] conformers via coordinating oxygen atoms in [BMB] anions. For a given alkali metal ion, both B(R)-Man(RR) and B(S)-Man(SS) [BMB] conformers have the most stable alkali metal ion-[BMB] binding structures, as verified from the relative binding energies shown in **Table 1**, due to the intrinsic V-shaped distributions of two phenyl groups in [BMB] anionic frameworks. All three alkali metal ions are intrinsically coordinated with B(R)-Man(RR) and B(S)-Man(SS) [BMB] conformers in local cavities of V-shaped conformations. For bent and twisted [BMB] conformers, alkali metal ions either coordinate with two oxygen atoms in central  $\text{BO}_4$  moieties or with one oxygen in  $\text{BO}_4$  moieties and the other one in C=O moieties depending on the delicate interactions of alkali metal ions with specific atoms in [BMB] conformers.

In addition, alkali metal ions have preferential associations with phenyl groups in V-shaped B(R)-Man(RR) and B(S)-Man(SS) [BMB] conformers. It is demonstrated that an increase of alkali metal ion sizes from  $\text{Li}^+$  to  $\text{Na}^+$  and  $\text{K}^+$  ions leads to their distinct cation- $\pi$  coordinations with phenyl groups (Dougherty, 2012). Larger alkali metal ions have stronger cation- $\pi$  interactions and therefore have larger binding energies with V-shaped B(R)-Man(RR) and B(S)-Man(SS) [BMB] conformers. This may lead to distinct applications of [BMB] anions in alkali metal ion batteries, in which alkali metal ion-[BMB] adducts are effective charge carriers contributing to significant ion conductivities in electrochemical devices.

Additional electronic properties of alkali metal ion-[BMB] complexes were calculated based on their optimized ion-pair structures. The energy levels of the highest occupied molecular orbital (HOMO) and the lowest unoccupied molecular orbital (LUMO) for the optimized Li[BMB] ion-pair structures are shown in **Figure 6**. According to the frontier molecular orbital theory, the HOMO and LUMO energies are useful for evaluating the electron-donating and -accepting abilities of ion species (Dong et al., 2012; García et al., 2015). Higher values of HOMO energy and lower values of LUMO energy indicate a larger tendency for ion species to donate and accept electrons, respectively. In addition, the HOMO and LUMO energies are directly related to ionization potential and electron affinity and give quantitative information on the possible electron transition between alkali metal ions and [BMB] anions. The energy difference between HOMO and LUMO is an important parameter determining the molecular-electrical transport properties, molecular stabilities, and liquid phase electrochemical windows of alkali metal ion-[BMB] complexes (Dong et al., 2012; García et al., 2015; Yllö and Zhang, 2019). It is shown that the HOMO and LUMO energy levels and energy gaps for the six Li[BMB] ion-pair complexes generally follow a similar tendency as the relative binding energies (listed in **Table 1**) for these [BMB] conformers in coordinating  $\text{Li}^+$  ions. The twisted B(R)-Man(SS) and B(S)-Man(RR) [BMB] conformers have the lowest energy gap among

the three categories, indicating that  $\text{Li}^+$  ions tend to have higher reactivities with twisted [BMB] configurations than with other [BMB] conformers. The energy gaps for bent B(R)-Man(RS) and B(S)-Man(SR) [BMB] conformers are slightly larger than those for twisted [BMB] configurations. It is noteworthy that for the two V-shaped structures, the Li[BMB] (B(S)-Man(SS)) ion pair has a larger energy gap than does the Li[BMB] (B(R)-Man(RR)) ion pair. This indicates that the Li[BMB] (B(S)-Man(SS)) ion pair has higher stability and opposing charge transfer than other Li[BMB] ion-pair structures, since this ion-pair complex opposes changes in its electron density and distribution. In addition, the Li[BMB] (B(S)-Man(SS)) ion-pair complex has a lower HOMO energy than the Li[BMB] (B(R)-Man(RR)) ion-pair structure, indicating that the former complex has a distinct electrochemical stability and a larger electrochemical window than other Li[BMB] ion-pair structures when it is used as a solvent electrolyte in Li-ion batteries (Franco et al., 2019; Nilsson-Hallén et al., 2019).

The computational HOMO and LUMO contours for the optimized Li[BMB] ion-pair structures are shown in **Figure 7**. It is clearly demonstrated that HOMO positions are mainly localized on phenyl groups and partially extended to oxalato ring structures for all Li[BMB] ion-pair complexes. This observation is attributed to the  $\pi$ -states of aromatic ring structures including both phenyl and oxalato ring moieties. However, the LUMO distributions are concentrated over  $\text{Li}^+$  ions for V-shaped B(S)-Man(SS) and B(R)-Man(RR) [BMB] conformers and are located primarily around  $\text{Li}^+$  ions and phenyl groups for twisted B(R)-Man(SS) and B(S)-Man(RR) [BMB] conformers as well as for bent B(R)-Man(RS) and B(S)-Man(SR) [BMB] conformers. The occurrence of electron transfer from HOMO to LUMO centers leads to an electron density transfer from one phenyl group to the other in the same anion framework via central oxalato moieties. Therefore, [BMB] anions are primarily responsible for the charge transfer process between  $\text{Li}^+$  ions and anions. Furthermore, we can assume that intramolecular charge transfer is enhanced within an anion framework for anions with larger ion hydrophobicity.

The HOMO and LUMO energy levels for the optimized Na[BMB] and K[BMB] ion-pair structures are shown in **Figure 8**. These HOMO and LUMO energies and energy gaps exhibit similar features as those for Li[BMB] ion-pair structures, indicating that these alkali metal ions have similar coordination patterns with [BMB] anions but with different interaction strength. In addition, the HOMO and LUMO contours for the optimized Na[BMB] and K[BMB] ion-pair structures shown in **Figures 9, 10** present a qualitative difference from those for the optimized Li[BMB] ion-pair complexes shown in **Figure 7** owing to the different ion parameters of  $\text{Li}^+$ ,  $\text{Na}^+$ , and  $\text{K}^+$  ions. Nevertheless, the distinct coordination patterns and interaction strengths of different [BMB] conformers with three alkali metal ions may lead to the varied stabilities and electrochemical windows of alkali metal ion-[BMB] complexes. These striking physicochemical properties may contribute to striking applications of [BMB] anions in alkali metal ion batteries, in which alkali metal ion-[BMB] complexes are effective charge carriers contributing to significant ion conductivities in electrochemical devices.

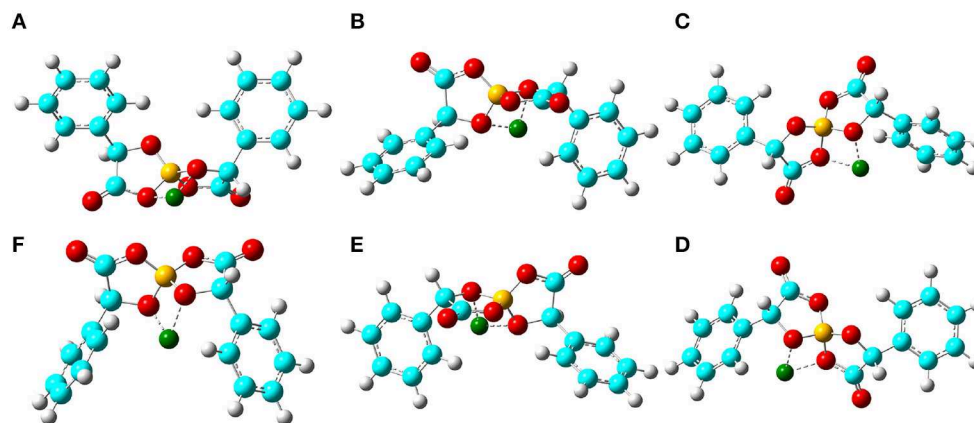


**FIGURE 3** | Optimized ion-pair structures of an  $\text{Li}^+$  ion in coordinating [BMB] anions with varied molecular chiralities determined from DFT calculations. The hydrogen, boron, carbon, and oxygen atoms in [BMB] anions are represented by white, yellow, cyan, and red spheres, respectively, and  $\text{Li}^+$  ions are represented by green spheres. **(A)** B(R)-Man(RR), **(B)** B(R)-Man(RS), **(C)** B(R)-Man(SS), **(D)** B(S)-Man(RR), **(E)** B(S)-Man(SR), and **(F)** B(S)-Man(SS).

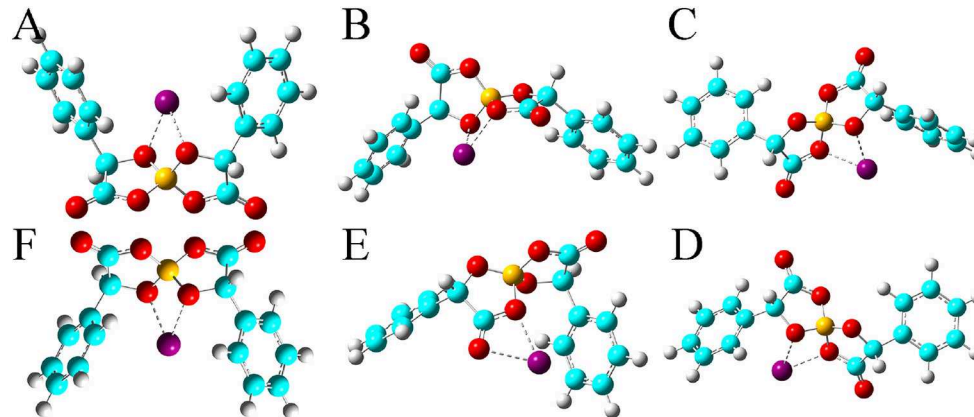


**FIGURE 4** | Optimized ion-pair structures of an  $\text{Na}^+$  ion in coordinating [BMB] anions with varied molecular chiralities determined from DFT calculations. The hydrogen, boron, carbon, and oxygen atoms in [BMB] anions are represented by white, yellow, cyan, and red spheres, respectively, and  $\text{Na}^+$  ions are represented by purple spheres. **(A)** B(R)-Man(RR), **(B)** B(R)-Man(RS), **(C)** B(R)-Man(SS), **(D)** B(S)-Man(RR), **(E)** B(S)-Man(SR), and **(F)** B(S)-Man(SS).

### 3. ATOMISTIC SIMULATIONS OF TETRAALKYLPHOSPHONIUM [BMB] IONIC LIQUIDS

#### 3.1. Atomistic Simulation Methodology

The atomistic force field parameters of tetraalkylphosphonium cations and [BMB] anions are taken from a force field systematically developed in our previous studies based on the AMBER framework (Wang et al., 2014, 2015b). The cross-interaction parameters between different atom types are obtained from the Lorentz-Berthelot combination rules. It is noteworthy that during force field development for tetraalkylphosphonium orthoborate ILs in our previous work (Wang et al., 2014), both tetraalkylphosphonium cations and orthoborate anions were described by unity charges and all atomic partial charges were determined by fitting the molecular electrostatic potential generated from DFT calculations of individual ions. In recent

computational studies, it has been suggested that a down-scaling of atomic partial charges is an effective way to account for polarization and charge transfer effects between ion species and thereby can improve the reliability of calculations of the dynamical and transport quantities of ILs (Morrow and Maginn, 2002; Ishizuka and Matubayasi, 2016). It was identified in a recent study that a charge scaling factor of 0.8 could provide liquid viscosities for  $[\text{P}_{6,6,6,14}][\text{BMB}]$  and  $[\text{P}_{6,6,6,14}]\text{Cl}$  ILs that were as reliable as those obtained from experimental measurements within a wide temperature interval of 373–463 K (Sarman et al., 2018). Therefore, in the current work, all atomic partial charges for atoms in tetraalkylphosphonium cations and [BMB] anions are uniformly rescaled using a scaling factor of 0.8. It should be noted that even though the adopted charge scaling factor of 0.8 is an empirical correction of electrostatic polarization and charge transfer effects between tetraalkylphosphonium cations and [BMB] anions, it gives good performance in

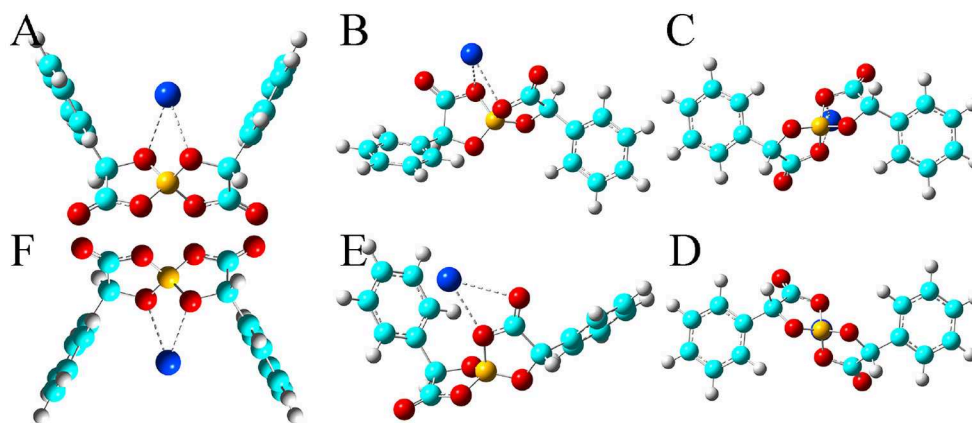


**FIGURE 5** | Optimized ion-pair structures of a  $K^+$  ion in coordinating [BMB] anions with varied molecular chiralities determined from DFT calculations. The hydrogen, boron, carbon, and oxygen atoms in [BMB] anions are represented by white, yellow, cyan, and red spheres, respectively, and  $K^+$  ions are represented by blue spheres. (A) B(R)-Man(RR), (B) B(R)-Man(RS), (C) B(R)-Man(SS), (D) B(S)-Man(RR), (E) B(S)-Man(SR), and (F) B(S)-Man(SS).

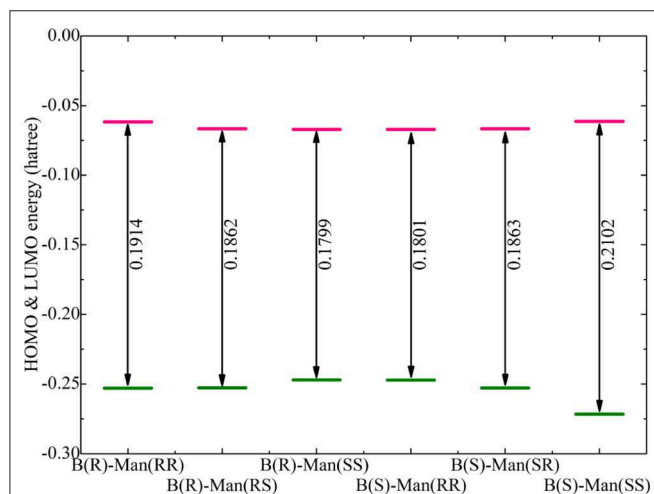


**FIGURE 6** | Computational HOMO and LUMO energies (in Hartree), and energy gaps (LUMO-HOMO) for Li[BMB] ion-pair complexes with anions of varied molecular chiralities. These computational results were obtained from DFT calculations at the B3LYP/6-311+G(d) level of theory with Grimme's-D3 dispersion correction.

describing the thermodynamics and microstructural quantities of tetraalkylphosphonium [BMB] ILs.

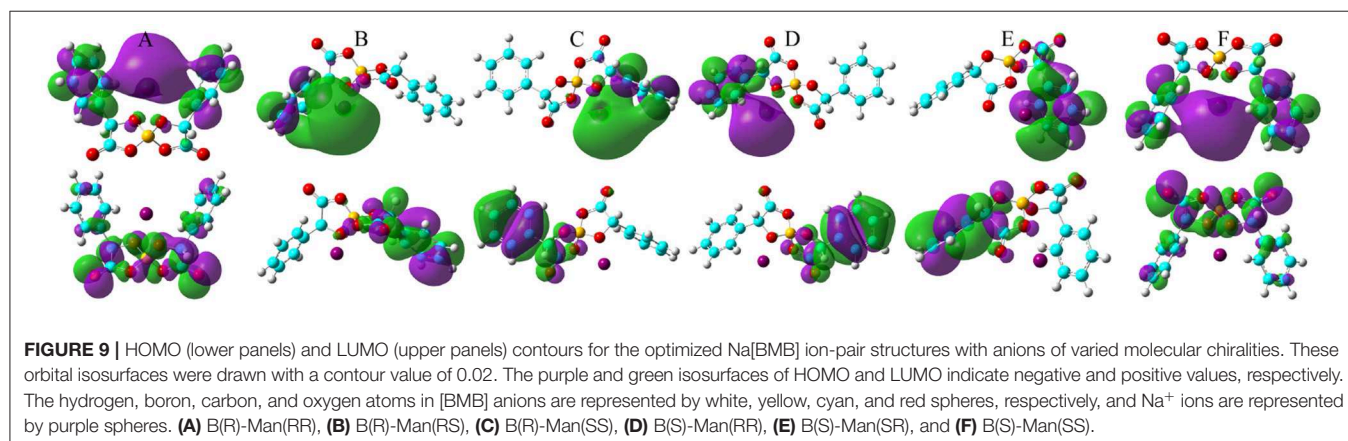
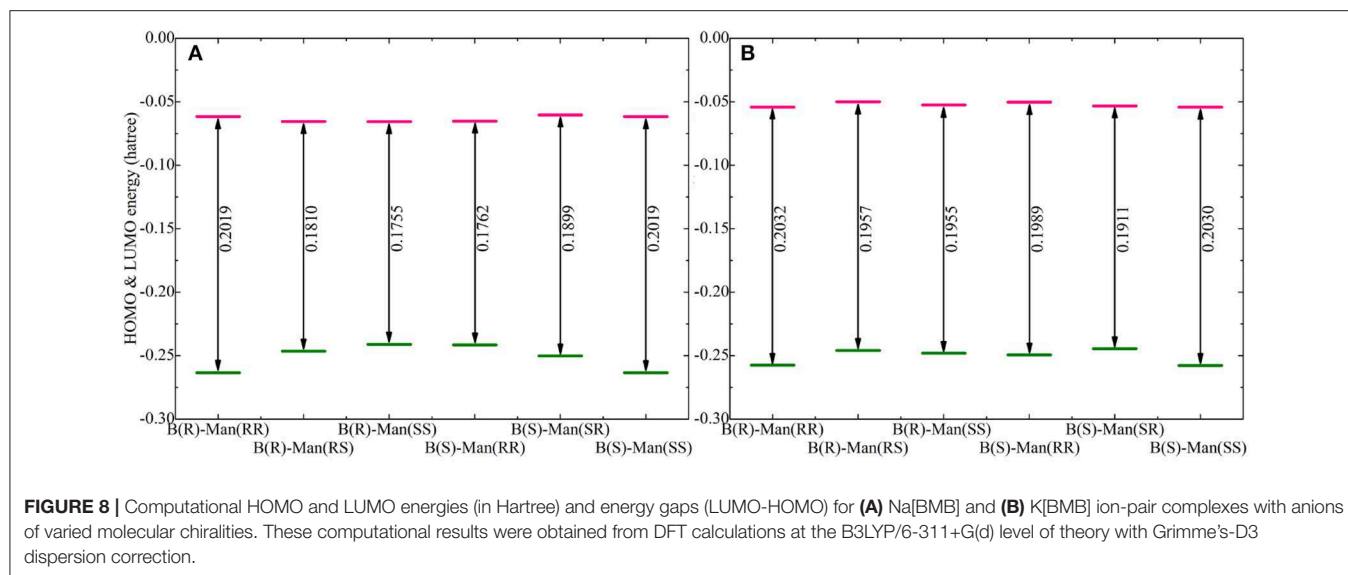
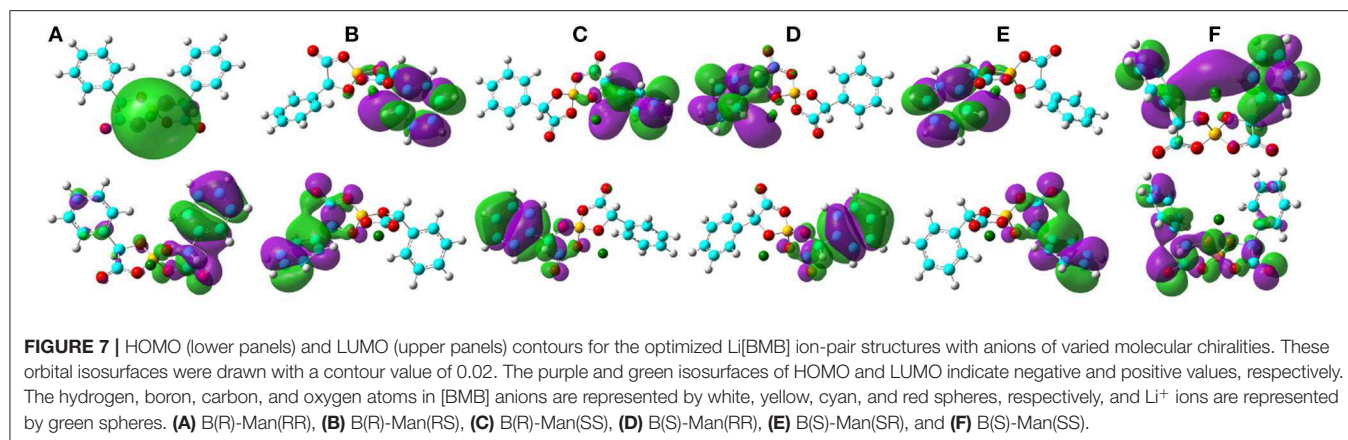
In present atomistic simulations, each simulation system consists of a varied number of tetraalkylphosphonium [BMB] ion pairs, having approximately 35,000 atoms. More specifically,  $[P_{4,4,4,4}][BMB]$ ,  $[P_{4,4,4,8}][BMB]$ , and  $[P_{6,6,6,14}][BMB]$  IL systems are composed of 400, 352, and 259 ion pairs, respectively. Atomistic simulations were performed using the GROMACS 5.0.7 package (Abraham et al., 2015) with cubic periodic boundary conditions. The equations of motion were integrated using a classical velocity Verlet leapfrog integration algorithm with a time step of 1.0 fs. A cutoff distance of 1.6 nm was set for short-range van der Waals interactions and real-space

electrostatic interactions between atomic partial charges. The Particle-Mesh Ewald summation method with an interpolation order of 5 and a Fourier grid spacing of 0.16 nm was employed to handle long-range electrostatic interactions in reciprocal space.

All tetraalkylphosphonium [BMB] IL systems were first energetically minimized using a steepest-descent algorithm and thereafter annealed gradually from 800 to 323 K within 20 ns. All annealed simulation systems were equilibrated in NPT (isothermal-isobaric) ensemble for 60 ns of physical time, maintained using Nosé-Hoover chain thermostat and Parrinello-Rahman barostat with time coupling constants of 0.5 and 0.2 ps, respectively, to control temperature at 323 K and pressure at 1 atm. Atomistic simulations of all simulation systems were further performed in NVT ensemble for 100 ns, and simulation trajectories were recorded at an interval of 100 fs for further microstructural analysis. Additional atomistic simulations were performed at a wide temperature range to address the dependence of the liquid densities of all studied tetraalkylphosphonium [BMB] ILs on temperature for comparative purposes.

### 3.2. Liquid Densities

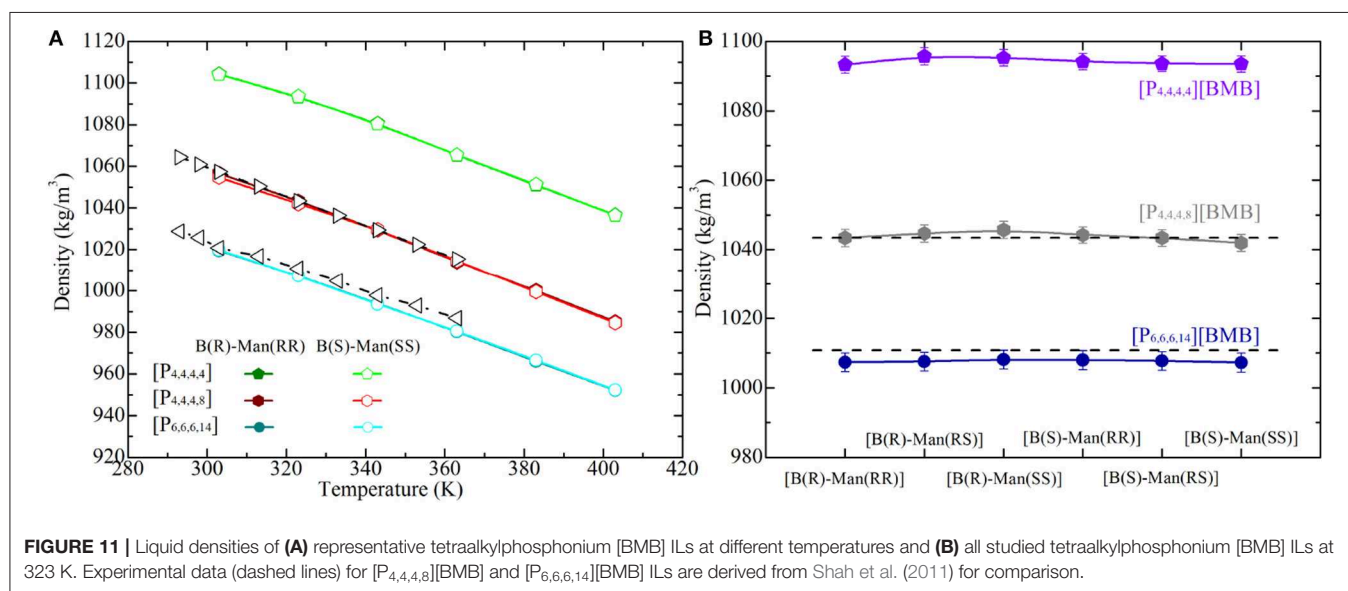
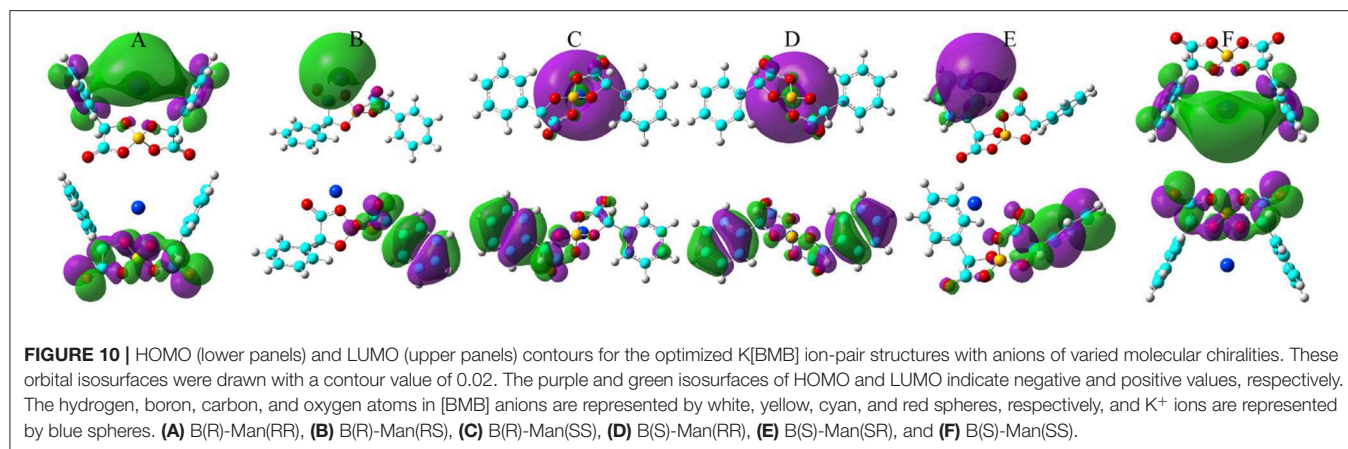
The liquid densities of all of the studied tetraalkylphosphonium [BMB] IL systems were calculated from current atomistic simulations at different temperatures ranging from 293 to 373 K with an interval of 20 K, and representative computational results are shown in **Figure 11**. In addition, experimental density data of  $[P_{4,4,4,8}][BMB]$  and  $[P_{6,6,6,14}][BMB]$  ILs taken from Shah et al. (2011) are also provided in **Figure 11** for comparative purposes. The liquid densities of all tetraalkylphosphonium [BMB] ILs exhibit linear variations as temperature changes within the investigated temperature range. For a given [BMB] conformer, both the experimental and computational density results of tetraalkylphosphonium [BMB] ILs decrease with increasing number of carbon atoms in cations at specific temperatures, following that order  $[P_{4,4,4,4}] > [P_{4,4,4,8}] >$



[P<sub>6,6,6,14</sub>]. This is attributed to the reduced interactions between large tetraalkylphosphonium cations and [BMB] anions leading to their less efficient packing in heterogeneous IL matrices (Wang et al., 2014, 2017b). In addition, a good agreement is observed between experimental data and

computational results for [P<sub>4,4,4,8</sub>][BMB] and [P<sub>6,6,6,14</sub>][BMB] ILs at all studied temperatures.

However, the molecular chiralities of [BMB] anions have a negligible effect on the liquid densities of these tetraalkylphosphonium [BMB] ILs, which may be attributable



to elaborate interactions among all constituent ions in liquid environments. It is known that liquid density is a thermodynamic manifestation of all possible ion pair and ion cluster structures in local liquid environments. Even though [BMB] conformers have their intrinsic molecular volumes, as determined from DFT calculations, these [BMB] anions have delicate coordinations with tetraalkylphosphonium cations in heterogeneous IL matrices, leading to their comparable liquid densities as shown in **Figure 11B**. In addition, the agreement between experimental data and simulation results is remarkably good, with a maximum deviation of approximately 0.3% and 0.5% for [P<sub>4,4,4,8</sub>][BMB] and [P<sub>6,6,6,14</sub>][BMB] ILs, respectively. These computational data suggest that there might be multiple [BMB] conformers in experimental tetraalkylphosphonium [BMB] IL samples depending on the relative ratio of R- and S-mandelic acids in the reaction vessel. Therefore, an advanced synthesis method and separation technology would be useful for better extraction of varied [BMB] conformers from IL samples due to their specific coordinations with cation groups like alkali metal ions.

### 3.3. Hydrogen Bonding Interactions

HB interactions between ion species in ILs are one of the most important interactions and have a significant effect on ion packing structures in local ionic environments (Hunt et al., 2015; Matthews et al., 2015; Sha et al., 2016; Wang et al., 2017a; Wang, 2018; Pei and Laaksonen, 2019; Wang et al., submitted). In the current work, we studied HB interactions between tetraalkylphosphonium cations and [BMB] anions with varied molecular chiralities. For all these tetraalkylphosphonium [BMB] ILs, HP atoms in cations (as labeled in **Figure 1**) are potential HB donor sites (Wang et al., 2017b; Wang et al., submitted), and all three oxygen atom types in anions (as labeled in **Figure 1**) are preferential HB acceptors.

**Figure 12** presents representative HP-O radial distribution functions (RDFs) for HB coordinations of tetraalkylphosphonium cations with [BMB] anions. For given tetraalkylphosphonium cations, the RDF peak intensities of HP atoms in coordinating OA and OB atoms in [BMB] anions follow the three categories of [BMB] conformers as discussed in the previous section. The V-shaped B(R)-Man(RR) and

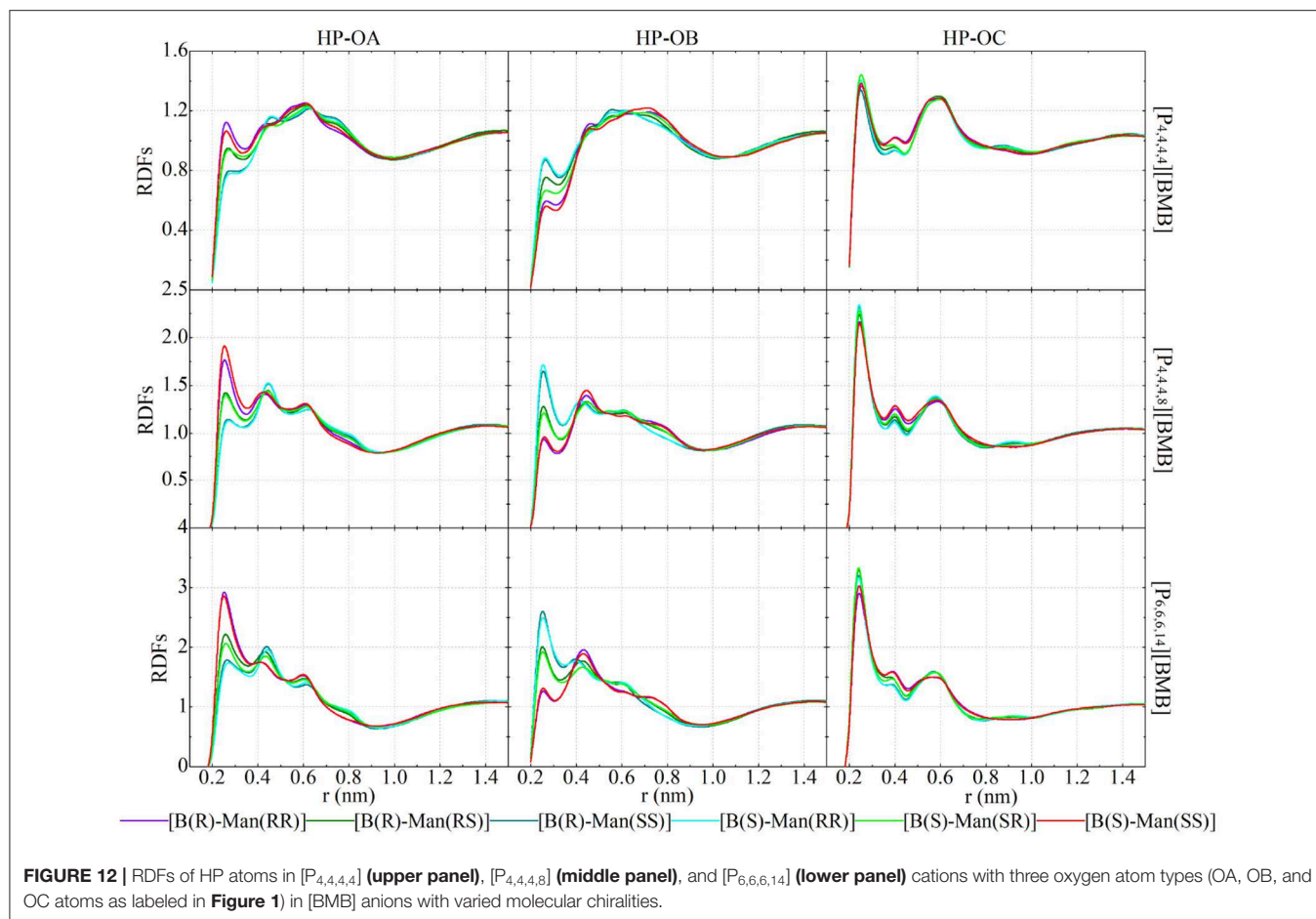


**FIGURE 12** | RDFs of HP atoms in  $[P_{4,4,4,4}]$  (upper panel),  $[P_{4,4,4,8}]$  (middle panel), and  $[P_{6,6,6,14}]$  (lower panel) cations with three oxygen atom types (OA, OB, and OC atoms as labeled in **Figure 1**) in [BMB] anions with varied molecular chiralities.

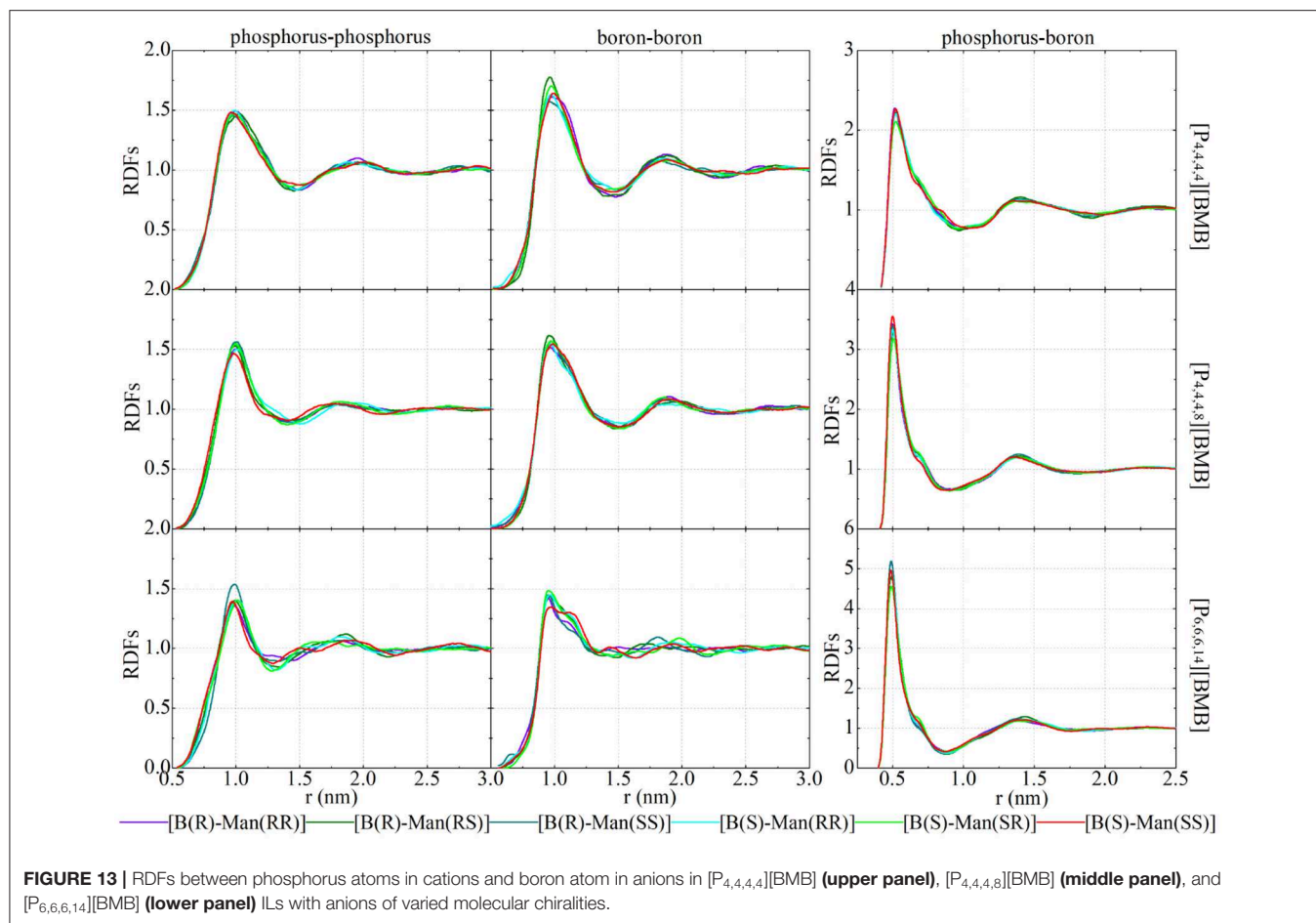
B(S)-Man(SS) [BMB] conformers have strong HB associations, the bent B(R)-Man(RS) and B(S)-Man(SR) [BMB] conformers have intermediate HB interactions, and the twisted B(R)-Man(SS) and B(S)-Man(RR) [BMB] conformers have weak HB coordinations with HP atoms in tetraalkylphosphonium cations via OA atoms (left column in **Figure 12**). However, an opposite effect is observed for HP atoms in HB interactions with OB atoms in [BMB] anions, as clearly manifested in the middle column of **Figure 12**. In addition, OC atoms in all [BMB] conformers have stronger interactions with HP atoms in tetraalkylphosphonium cations than OA and OB atoms, irrespective of the molecular chiralities of [BMB] conformers, as shown in the right column of **Figure 12**. These computational results indicate that OA and OB have competitive HB interactions with HP atoms in tetraalkylphosphonium cations and that their HB capabilities depend on the molecular chiralities, conformational flexibilities, and steric hindrance effects of [BMB] conformers. The V-shaped B(R)-Man(RR) and B(S)-Man(SS) [BMB] conformers have small cavities in phenyl-oxalato-phenyl domains, which prevent central polar groups of tetraalkylphosphonium cations from approaching, and thus OB atoms in local cavities have weak HP-OB interactions. The HB acceptor sites outside cavities, such as OC and OA atoms, have preferential HB interactions with HP atoms in tetraalkylphosphonium cations. For bent B(R)-Man(RS) and

B(S)-Man(SR) [BMB] conformers, both two OA and two OB atoms have one site inside and one outside local cavities, and thus OA and OB atoms have comparable HB associations with neighboring tetraalkylphosphonium cations via HP atoms. The OA and OB atoms have opposite distributions in twisted B(R)-Man(SS) and B(S)-Man(RR) [BMB] conformers to in V-shaped B(R)-Man(RR) and B(S)-Man(SS) [BMB] conformers, and thus they have distinct HB coordinations with tetraalkylphosphonium cations via HP atoms.

Enlarging tetraalkylphosphonium cation sizes from  $[P_{4,4,4,4}]$  (upper panels in **Figure 12**) to  $[P_{4,4,4,8}]$  (middle panels in **Figure 12**) and  $[P_{6,6,6,14}]$  (lower panels in **Figure 12**) leads to enhanced HB interactions of HP in cations with all three oxygen atom types in [BMB] anions. This observation is explained by enhanced segregation of polar groups consisting of central oxalato moieties in anions and central  $P(CH_2)_4$  groups in cations in apolar networks consisting of phenyl groups in anions and remaining alkyl moieties in cations with a gradual addition of apolar alkyl groups to tetraalkylphosphonium cations, as has been intensively discussed in previous works (Wang et al., 2017b; Wang, 2018).

### 3.4. Microscopic Liquid Structures

**Figure 13** esentative site-site RDFs of cation-cation, anion-anion, and cation-anion pairs for all of the studied



tetraalkylphosphonium [BMB] ILs. The central phosphorus atoms in tetraalkylphosphonium cations and boron atoms in [BMB] anions are taken as reference sites to calculate these RDFs, which are useful for depicting microscopic liquid structures between ion species in tetraalkylphosphonium [BMB] ILs. Both phosphorus-phosphorus and boron-boron RDF plots present very broad peaks at around 1.0 nm, with similar peak intensities in all of the studied tetraalkylphosphonium [BMB] ILs. The molecular chiralities of [BMB] anions have minimal effect on the spatial distributions of boron atoms in [BMB] anions around phosphorus atoms in tetraalkylphosphonium cations, and *vice versa*. These computational data are explained by strong Coulombic interactions among phosphorus and boron atoms in tetraalkylphosphonium cations and [BMB] anions, respectively. In addition, Coulombic interactions between central polar groups in tetraalkylphosphonium cations and [BMB] anions are overwhelmingly stronger than preferential intermolecular HB interactions, the latter of which have difficulty mediating the distributions of anions around cations but do fine-tune the local orientations of [BMB] conformers to maximize their HB interactions with tetraalkylphosphonium cations in local ionic environments.

Enlarging molecular sizes of tetraalkylphosphonium cations from [P<sub>4,4,4,4</sub>] (upper panels in **Figure 13**) to [P<sub>4,4,4,8</sub>] (middle

panels in **Figure 13**) and [P<sub>6,6,6,14</sub>] (lower panels in **Figure 13**) leads to increased intermolecular interactions between phosphorus and boron atoms in respective ion groups, as clearly manifested in the right column of **Figure 13**, owing to enhanced segregation of polar groups in apolar networks in heterogeneous IL matrices (Wang et al., 2017b; Wang, 2018).

In addition, we calculated the total X-ray scattering structural function,  $S(q)$ , using a summation of atom type-based partial components as  $S(q) = \sum_{i=1}^n \sum_{j=1}^n S_{ij}(q)$ , to explore the overall effect of the molecular chiralities of [BMB] anions and variations of tetraalkylphosphonium cation structures on microstructural ordering characteristics in tetraalkylphosphonium [BMB] ILs.  $S_{ij}(q)$  is a partial structural function between atom types  $i$  and  $j$  and is given by

$$S_{ij}(q) = \frac{\rho_0 x_i x_j f_i(q) f_j(q) \int_0^{L/2} 4\pi r^2 [g_{ij}(r) - 1] \frac{\sin(qr)}{qr} W(r) dr}{[\sum_{i=1}^n x_i f_i(q)]^2}$$

$x_i$  and  $x_j$  are mole fractions, and  $f_i(q)$  and  $f_j(q)$  are X-ray atomic form factors of atom types  $i$  and  $j$  in simulation systems (Prince and Wilson, 2004), respectively.  $g_{ij}(r)$  is the partial RDF between atom types  $i$  and  $j$ , including both intra- and intermolecular pairs.  $\rho_0 = \frac{N_{atom}}{\langle L^3 \rangle}$  refers to an averaged atom number density of a simulation system, and  $L$  is the simulation box length.  $W(r)$  is

a Lorch window function defined as  $W(r) = \frac{\sin(2\pi r/L)}{2\pi r/L}$ , which is used to minimize the effect of finite truncation of  $r$  for the calculation of  $g_{ij}(r)$ . For a simulation system of moderate size, this window function does not alter the physical meaning of peaks and anti-peaks in  $S(q)$  plots (Annapureddy et al., 2010; Hettige et al., 2012; Wu et al., 2016; Wang et al., 2017b).

**Figure 14A** presents the total X-ray scattering structural functions  $S(q)$  for  $[P_{4,4,4,4}][BMB]$  ILs in the range of  $q \leq 2.75 \text{ nm}^{-1}$ , which is the most relevant region and is associated with intermolecular correlations between tetraalkylphosphonium cations and [BMB] anions in heterogeneous IL matrices. Features at  $q$  values larger than  $2.75 \text{ nm}^{-1}$  are mostly intramolecular in nature, which are fairly easy to assign and thus are not discussed in the current work. Two prominent peaks located at  $\sim 0.76 \text{ nm}^{-1}$  and  $\sim 1.51 \text{ nm}^{-1}$  are shown in these total X-ray scattering structural functions for  $[P_{4,4,4,4}][BMB]$  ILs with anions of varied molecular chiralities. Such a two-peak-plot is a general feature for tetraalkylphosphonium ILs and is mainly attributed to the bulky and voluminous structures of cations and their strong coordinations with anions via strong Coulombic interactions between polar groups in the respective ion species and preferential hydrophobic interactions among alkyl and phenyl moieties in the constituent ions (Amith et al., 2016; Hettige et al., 2016; Wang et al., 2017b; Wang et al., submitted). These peak positions are essential characteristic hallmarks of their microstructural landscapes, indicating particular microscopic ion ordering phenomena at different length scales in tetraalkylphosphonium [BMB] IL matrices (Annapureddy et al., 2010; Hettige et al., 2012; Amith et al., 2016; Wu et al., 2016; Wang et al., 2017b; Wang, 2018; Wang et al., submitted).

The peaks in the intermediate  $q$  range around  $0.76 \text{ nm}^{-1}$  are indicative of a mesoscopic liquid organization

characterized by positive-negative charge alternations in IL matrices (Canongia Lopes and Pádua, 2006; Annapureddy et al., 2010; Amith et al., 2016; Wu et al., 2016; Wang et al., 2017b; Weyman et al., 2018; Wang et al., submitted). This charge ordering behavior results from the need to maintain a lattice-like arrangement of cations and anions to minimize Coulombic interactions in IL matrices and is thus associated with a length scale between ions of the same charge separated by ions of opposite charge (Annapureddy et al., 2010; Hettige et al., 2012; Wu et al., 2016; Wang et al., 2017b; Wang, 2018; Weyman et al., 2018; Wang et al., submitted). For some ILs, this charge alternation peak is present as a weak shoulder because of an almost complete cancellation of peaks and anti-peaks, which offsets this ordering phenomena at intermediate length scale (Amith et al., 2016; Wang et al., 2017b). The prominent peaks at high  $q$  values near  $1.51 \text{ nm}^{-1}$  are associated with short-range adjacency correlations originating from the nearest neighboring ion species (Annapureddy et al., 2010; Hettige et al., 2012, 2016; Wu et al., 2016; Wang et al., 2017b; Wang, 2018; Wang et al., submitted). In fact, this peak mainly originates from apolar adjacency correlations between ion species, as has been verified in previous studies (Hettige et al., 2012; Amith et al., 2016; Wu et al., 2016; Wang et al., 2017b; Weyman et al., 2018).

Either for the total X-ray scattering structural functions or the partial structural functions for cation-anion/anion-cation (**Figure 14B**), cation-cation (**Figure 14C**), and anion-anion (**Figure 14D**) subcomponents in  $[P_{4,4,4,4}][BMB]$  ILs, the dependence of charge alternations and adjacency correlations in these scattering structural functions on the molecular chiralities of [BMB] anions is negligible. This is expected, as scattering structural functions are intrinsically determined by RDFs between different atom pairs. It is shown in **Figure 13** that

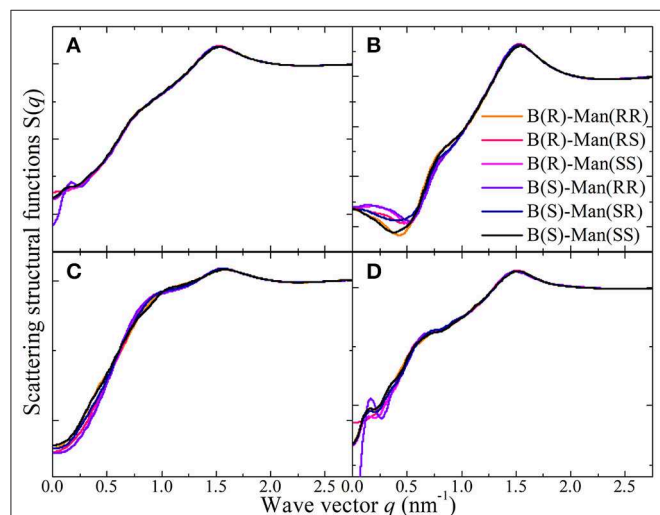


**FIGURE 14 | (A)** The total X-ray scattering structural functions  $S(q)$  in the range of  $q \leq 2.75 \text{ nm}^{-1}$  for  $[P_{4,4,4,4}][BMB]$  IL at 323 K with anions of varied molecular chiralities. These total X-ray scattering structural functions are further partitioned into partial structural functions for **(B)** cation-anion/anion-cation, **(C)** cation-cation, and **(D)** anion-anion subcomponents.

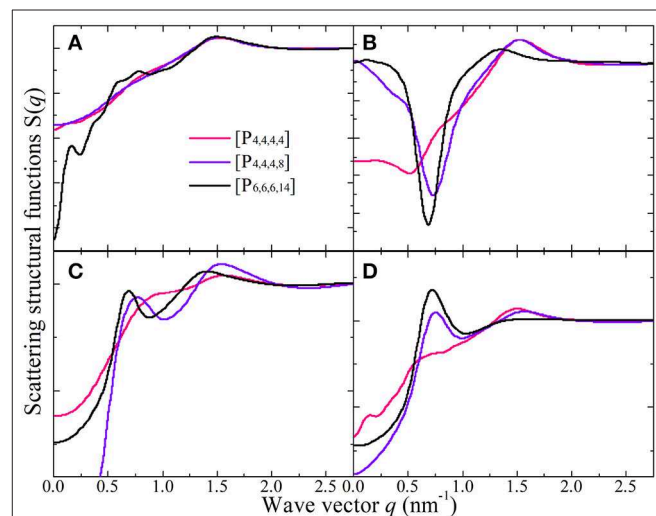
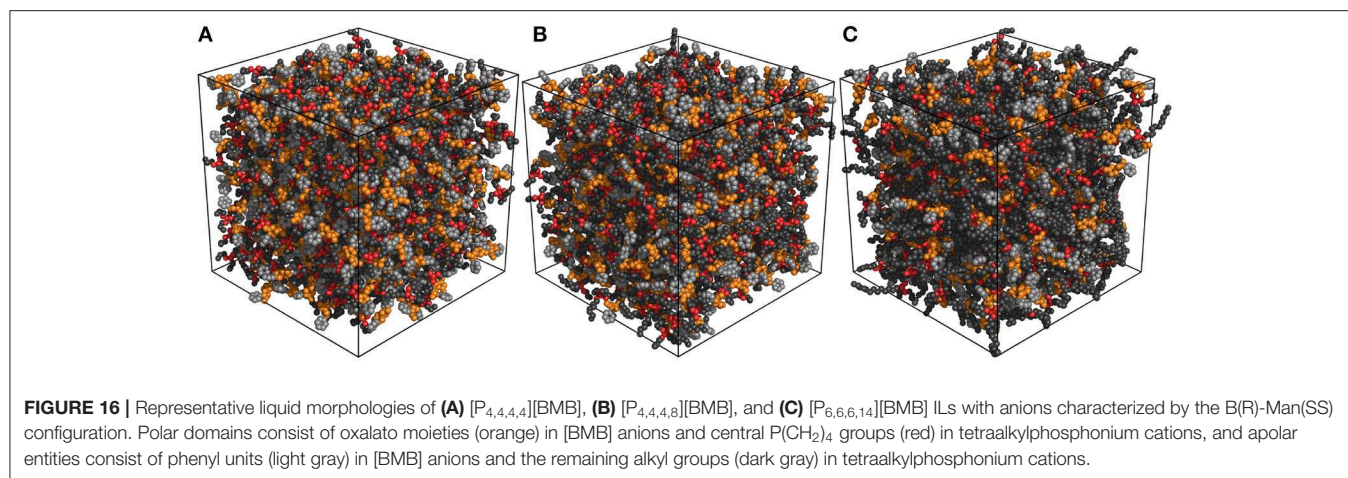


**FIGURE 15 | (A)** The total X-ray scattering structural functions  $S(q)$  in the range of  $q \leq 2.75 \text{ nm}^{-1}$  for tetraalkylphosphonium [BMB] ILs at 323 K with anions characterized by the B(R)-Man(SS) configuration. These total X-ray scattering structural functions are further partitioned into partial structural functions for **(B)** cation-anion/anion-cation, **(C)** cation-cation, and **(D)** anion-anion subcomponents.



the molecular chiralities of [BMB] anions have minimal effects on phosphorus-phosphorus, phosphorus-boron, and boron-boron RDFs, which leads to comparable scattering structural functions for  $[P_{4,4,4,4}][BMB]$  ILs with anions of varied molecular chiralities. Therefore, it can be asserted that  $[P_{4,4,4,4}][BMB]$  ILs are characterized by similar liquid morphologies, which are independent of the molecular chiralities of [BMB] anions. Additional computational results indicating that the molecular chiralities of [BMB] anions have minimal influence on the total and partial scattering structural functions were also obtained for  $[P_{4,4,4,8}][BMB]$  and  $[P_{6,6,6,14}][BMB]$  ILs.

**Figure 15** presents representative total and partial X-ray scattering structural functions for tetraalkylphosphonium [BMB] ILs at 323 K with anions characterized by the B(R)-Man(SS) configuration. In the intermediate  $q$  range, both cation-cation (**Figure 15C**) and anion-anion (**Figure 15D**) subcomponents contribute to positive intensities, and the cross-term cation-anion/anion-cation subcomponent (**Figure 15B**) exhibits prominent anti-peaks in the same  $q$  range. A combination of these peaks and anti-peaks contributes to prominent peaks registered in the intermediate  $q$  range in the total X-ray scattering structural functions shown in **Figure 15A**. Independent of tetraalkylphosphonium [BMB] ILs, the charge alternation peaks always appear as a result of the cancellation of prominent positive contributions from same-charge subcomponents and distinct negative-going peaks from cross-term contributions (Annapureddy et al., 2010; Amith et al., 2016; Wu et al., 2016; Wang et al., 2017b; Wang, 2018; Weyman et al., 2018). This observation indicates that, at specific locations where one expects to find a same-charge ion, there is a systematic absence of ions with opposite charge (Annapureddy et al., 2010; Hettige et al., 2012, 2016; Amith et al., 2016; Wu et al., 2016; Wang et al., 2017b; Wang, 2018; Wang et al., submitted). In addition, all partial scattering structural functions present positive contributions to adjacency correlations between neighboring ion species at high  $q$  values around  $1.51 \text{ nm}^{-1}$  but with different portions of contribution.

Different to the effect of the molecular chiralities of [BMB] anions on the scattering structural functions for

tetraalkylphosphonium [BMB] ILs, the variation of cation structures from  $[P_{4,4,4,4}]$  to  $[P_{4,4,4,8}]$  and  $[P_{6,6,6,14}]$  has a significant effect on RDFs (**Figure 13**), scattering structural functions (**Figure 15**), and microscopic liquid morphologies (**Figure 16**). Enlarging cation sizes from  $[P_{4,4,4,8}]$  to  $[P_{6,6,6,14}]$  leads to a concomitant shift of scattering peaks for charge alternations and adjacency correlations to lower  $q$  values (corresponding to larger characteristic distances for apolar domains in real space) in total and partial scattering structural functions (Amith et al., 2016; Wu et al., 2016; Wang et al., 2017b; Wang, 2018; Wang et al., submitted). These computational results are explained by dispersed distributions of polar domains consisting of central oxalato moieties in anions and central  $P(CH_2)_4$  groups in cations in apolar networks consisting of phenyl groups in anions and remaining alkyl moieties in cations and also the expansion of apolar networks in IL matrices with lengthening alkyl chains in tetraalkylphosphonium cations, as shown in **Figure 16**. Such a microstructural change in tetraalkylphosphonium [BMB] IL matrices has an impact on the number of counterions present in the solvation shells of a given ion and an even bigger effect on the distributions of (same-charge) ions nearby and thus contributes to distinct changes in peak positions for charge alternations and adjacency correlations at low and high  $q$  values, respectively. This observation is, in general, consistent with computational results for imidazolium oxalato borate ILs with cations with varied alkyl chains (Wang et al., 2017a; Wang, 2018) and for ILs consisting of tetraalkylphosphonium cations coupled with chloride, bromide, dicyanamide, and bis(trifluoromethylsulfonyl)imide anions (Hettige et al., 2012, 2016; Wang et al., 2017b; Wang et al., submitted).

#### 4. CONCLUDING REMARKS

Spiroborate anion-based inorganic electrolytes and ILs have fascinating physicochemical and structural properties and have promising applications in tribology and electrochemistry. Besides variations in cation structures, the molecular chiralities of spiroborate anions have a significant effect on their

macroscopic functionalities in these applications due to their specific binding structures and preferential interactions with neighboring ions in liquid matrices. A thorough understanding of the delicate associations between spiroborate anions and the paired cation species will provide valuable information for the selection and design of suitable lubricants and solvent electrolytes with desirable physicochemical properties for their specific applications.

In the current study, we performed intensive DFT calculations to study the specific binding structures of [BMB] anions with varied molecular chiralities with representative alkali metal ions and the representative electronic properties of the alkali metal ion-[BMB] ion pair complexes. The optimized [BMB] conformers are characterized by V-shaped, bent, and twisted anion structures with varied electrostatic potential contours, conformational energies, and distinct alkali metal ion-[BMB] binding structures. Alkali metal ions have considerable associations with phenyl groups in V-shaped [BMB] conformers owing to preferential cation- $\pi$  interactions.

In addition, we carried out extensive atomistic interactions to explore the effects of the molecular chiralities of [BMB] anions on the thermodynamics and microstructural properties of bulk tetraalkylphosphonium [BMB] ILs. It was revealed that oxygen atoms in [BMB] anions have competitive hydrogen bonding interactions with hydrogen atoms in tetraalkylphosphonium cations depending on the molecular chiralities of [BMB] anions and the steric hindrance effects of phenyl groups in [BMB] anions. However, the molecular chiralities of [BMB] anions have little effect on the liquid densities of tetraalkylphosphonium [BMB] ILs and the spatial distributions of boron atoms in anions around phosphorous atoms in cations. Enlarging tetraalkylphosphonium cation sizes from [P<sub>4,4,4,4</sub>] to [P<sub>4,4,4,8</sub>] and [P<sub>6,6,6,14</sub>] leads to enhanced cation-anion intermolecular hydrogen bonding and Coulombic interactions, as well as to distinct microscopic liquid structures as characterized by computational X-ray scattering structural functions, due to

enhanced segregation of polar groups (consisting of central oxalato moieties in [BMB] anions and central P(CH<sub>2</sub>)<sub>4</sub> groups in tetraalkylphosphonium cations) in apolar networks (composed of phenyl groups in [BMB] anions and the remaining alkyl moieties in tetraalkylphosphonium cations) in heterogeneous IL matrices.

## DATA AVAILABILITY STATEMENT

The raw data supporting the conclusions of this article will be made available by the authors, without undue reservation, to any qualified researcher.

## AUTHOR CONTRIBUTIONS

Y-LW designed DFT and atomistic simulations and performed DFT calculations. H-WP performed atomistic simulations. All authors wrote, reviewed, and edited all versions of this article.

## FUNDING

This work was supported by Knut and Alice Wallenberg Foundation, Swedish Science Council, and Ministry of Research and Innovation (Romania).

## ACKNOWLEDGMENTS

Y-LW gratefully acknowledges financial support from the Knut and Alice Wallenberg Foundation. AL acknowledges the Swedish Science Council for financial support and thanks a grant from the Ministry of Research and Innovation, CNCS-UEFISCDI, project number PN-III-P4-ID-PCCF-2016-0050, within PNCDI III, for partial support. All molecular simulations were performed using computational resources provided by the Swedish National Infrastructure for Computing (SNIC) at PDC, HPC2N, and NSC.

## REFERENCES

- Abbott, A. P., Frisch, G., and Ryder, K. S. (2013). Electroplating using ionic liquids. *Annu. Rev. Mater. Res.* 43, 335–358. doi: 10.1146/annurev-matsci-071312-121640
- Abraham, M. J., Murtola, T., Schulz, R., Páll, S., Smith, J. C., Hess, B., et al. (2015). Gromacs: high performance molecular simulations through multi-level parallelism from laptops to supercomputers. *SoftwareX* 1, 19–25. doi: 10.1016/j.softx.2015.06.001
- Absalan, G., Alipour, Y., Rezaei, Z., and Akhond, M. (2012). Determination of enantiomer compositions of propranolol enantiomers by chiral ionic liquid as a chiral selector and the uv-assisted spectrophotometric method. *Anal. Methods* 4, 2283–2287. doi: 10.1039/c2ay25161b
- Amith, W. D., Hettige, J. J., Castner, E. W. Jr., and Margulis, C. J. (2016). Structures of ionic liquids having both anionic and cationic octyl tails: Lamellar vacuum interface vs sponge-like bulk order. *J. Phys. Chem. Lett.* 7, 3785–3790. doi: 10.1021/acs.jpcclett.6b01763
- An, R., Zhou, G., Zhu, Y., Zhu, W., Huang, L., and Shah, F. U. (2018). Friction of ionic liquid-glycol ether mixtures at titanium interfaces: negative load dependence. *Adv. Mater. Interfaces* 5:1800263. doi: 10.1002/admi.201800263
- Annapureddy, H. V., Kashyap, H. K., De Biase, P. M., and Margulis, C. J. (2010). What is the origin of the prepeak in the x-ray scattering of imidazolium-based room-temperature ionic liquids? *J. Phys. Chem. B* 114, 16838–16846. doi: 10.1021/jp108545z
- Armand, M., Endres, F., MacFarlane, D. R., Ohno, H., and Scrosati, B. (2009). Ionic-liquid materials for the electrochemical challenges of the future. *Nat. Mater.* 8, 621–629. doi: 10.1038/nmat2448
- Bedrov, D., Piquemal, J.-P., Borodin, O., MacKerell, A. D. Jr., Roux, B., and Schroder, C. (2019). Molecular dynamics simulations of ionic liquids and electrolytes using polarizable force fields. *Chem. Rev.* 119, 7940–7995. doi: 10.1021/acs.chemrev.8b00763
- Boys, S. F., and Bernardi, F. D. (1970). The calculation of small molecular interactions by the differences of separate total energies. Some procedures with reduced errors. *Mol. Phys.* 19, 553–566. doi: 10.1080/00268977000101561
- Canongia Lopes, J. N., and Pádua, A. A. (2006). Nanostructural organization in ionic liquids. *J. Phys. Chem. B* 110, 3330–3335. doi: 10.1021/jp056006y
- Castner, E. W. Jr., Margulis, C. J., Maroncelli, M., and Wishart, J. F. (2011). Ionic liquids: structure and photochemical reactions. *Annu. Rev. Phys. Chem.* 62, 85–105. doi: 10.1146/annurev-physchem-032210-103421

- Dai, C., Zhang, J., Huang, C., and Lei, Z. (2017). Ionic liquids in selective oxidation: catalysts and solvents. *Chem. Rev.* 117, 6929–6983. doi: 10.1021/acs.chemrev.7b00030
- Dong, K., Song, Y., Liu, X., Cheng, W., Yao, X., and Zhang, S. (2012). Understanding structures and hydrogen bonds of ionic liquids at the electronic level. *J. Phys. Chem. B* 116, 1007–1017. doi: 10.1021/jp205435u
- Dougherty, D. A. (2012). The cation- $\pi$  interaction. *Acc. Chem. Res.* 46, 885–893. doi: 10.1021/ar300265y
- Franco, A. A., Rucci, A., Brandell, D., Frayret, C., Gaberscek, M., Jankowski, P., et al. (2019). Boosting rechargeable batteries r&d by multiscale modeling: myth or reality? *Chem. Rev.* 119, 4569–4627. doi: 10.1021/acs.chemrev.8b00239
- Frisch, M. J., Trucks, G. W., Schlegel, H. B., Scuseria, G. E., Robb, M. A., Cheeseman, J. R., et al. (2009). *Gaussian 09, Revision d. 01*. Wallingford, CT: Gaussian.
- García, G., Atilhan, M., and Aparicio, S. (2015). Adsorption of choline benzoate ionic liquid on graphene, silicene, germanene and boron-nitride nanosheets: a DFT perspective. *Phys. Chem. Chem. Phys.* 17, 16315–16326. doi: 10.1039/C5CP02432C
- Grimme, S., Antony, J., Ehrlich, S., and Krieg, H. (2010). A consistent and accurate ab initio parametrization of density functional dispersion correction (dft-d) for the 94 elements h-pu. *J. Chem. Phys.* 132:154104. doi: 10.1063/1.3382344
- Gusain, R., Bakshi, P. S., Panda, S., Sharma, O. P., Gardas, R., and Khatri, O. P. (2017). Physicochemical and tribophysical properties of trioctylalkylammonium bis (salicylate) borate (n888 n-bscb) ionic liquids: effect of alkyl chain length. *Phys. Chem. Chem. Phys.* 19, 6433–6442. doi: 10.1039/C6CP05990B
- Hayes, R., Warr, G. G., and Atkin, R. (2015). Structure and nanostructure in ionic liquids. *Chem. Rev.* 115, 6357–6426. doi: 10.1021/cr500411q
- Hettige, J. J., Araque, J. C., Kashyap, H. K., and Margulis, C. J. (2016). Nanoscale structure of tetradecyltriethylphosphonium based ionic liquids. *J. Chem. Phys.* 144:121102. doi: 10.1063/1.4944678
- Hettige, J. J., Kashyap, H. K., Annappureddy, H. V., and Margulis, C. J. (2012). Anions, the reporters of structure in ionic liquids. *J. Phys. Chem. Lett.* 4, 105–110. doi: 10.1021/jz301866f
- Hjalmarsson, N., Bergendal, E., Wang, Y.-L., Munavirov, B., Wallinder, D., Glavatskih, S., et al. (2019). Electro-responsive surface composition and kinetics of an ionic liquid in a polar oil. *Langmuir* 35, 15692–15700. doi: 10.1021/acs.langmuir.9b02119
- Hunt, P. A., Ashworth, C. R., and Matthews, R. P. (2015). Hydrogen bonding in ionic liquids. *Chem. Soc. Rev.* 44, 1257–1288. doi: 10.1039/C4CS00278D
- Ishizuka, R., and Matubayasi, N. (2016). Self-consistent determination of atomic charges of ionic liquid through a combination of molecular dynamics simulation and density functional theory. *J. Chem. Theory Comput.* 12, 804–811. doi: 10.1021/acs.jctc.5b00885
- Jankowski, P., Wiecezorek, W., and Johansson, P. (2016). New boron based salts for lithium-ion batteries using conjugated ligands. *Phys. Chem. Chem. Phys.* 18, 16274–16280. doi: 10.1039/C6CP02409B
- Kashyap, H. K., Santos, C. S., Daly, R. P., Hettige, J. J., Murthy, N. S., Shirota, H., et al. (2013). How does the ionic liquid organizational landscape change when nonpolar cationic alkyl groups are replaced by polar isoelectronic diethers? *J. Phys. Chem. B* 117, 1130–1135. doi: 10.1021/jp311032p
- Lee, C., Yang, W., and Parr, R. G. (1988). Development of the colle-salvetti correlation-energy formula into a functional of the electron density. *Phys. Rev. B* 37:785. doi: 10.1103/PhysRevB.37.785
- Matthews, R. P., Welton, T., and Hunt, P. A. (2015). Hydrogen bonding and  $\pi$ - $\pi$  interactions in imidazolium-chloride ionic liquid clusters. *Phys. Chem. Chem. Phys.* 17, 14437–14453. doi: 10.1039/C5CP00459D
- Morrow, T. I., and Maginn, E. J. (2002). Molecular dynamics study of the ionic liquid 1-n-butyl-3-methylimidazolium hexafluorophosphate. *J. Phys. Chem. B* 106, 12807–12813. doi: 10.1021/jp0267003
- Nilsson-Hallén, J., Ahlström, B., Marczewski, M., and Johansson, P. (2019). Ionic liquids: a simple model to predict ion conductivity based on dft derived physical parameters. *Front. Chem.* 7:126. doi: 10.3389/fchem.2019.00126
- Pei, H.-W., and Laaksonen, A. (2019). Feature vector clustering molecular pairs in computer simulations. *J. Comput. Chem.* 40, 2539–2549. doi: 10.1002/jcc.26028
- Pilkington, G. A., Harris, K., Bergendal, E., Reddy, A. B., Palsson, G. K., Vorobiev, A., et al. (2018). Electro-responsivity of ionic liquid boundary layers in a polar solvent revealed by neutron reflectance. *J. Chem. Phys.* 148:193806. doi: 10.1063/1.5001551
- Prince, E., and Wilson, A. J. C. (2004). *International Tables for Crystallography*. Kluwer Academic Publishers.
- Rohlmann, P., Munavirov, B., Furó, I., Antzutkin, O., Glavatskih, S., and Rutland, M. W. (2019). Non-halogenated ionic liquid dramatically enhances tribological performance of biodegradable oils. *Front. Chem.* 7:98. doi: 10.3389/fchem.2019.00098
- Sarman, S., Wang, Y.-L., Rohlmann, P., Glavatskih, S., and Laaksonen, A. (2018). Rheology of phosphonium ionic liquids: a molecular dynamics and experimental study. *Phys. Chem. Chem. Phys.* 20, 10193–10203. doi: 10.1039/C7CP08349A
- Sedghamiz, T., and Bahrami, M. (2019). Chiral ionic liquid interface as a chiral selector for recognition of propranolol enantiomers: a molecular dynamics simulations study. *J. Mol. Liq.* 292:111441. doi: 10.1016/j.molliq.2019.111441
- Sedghamiz, T., Ghalami, F., Sedghamiz, E., and Bahrami, M. (2018). Chiral recognition of propranolol enantiomers by chiral ionic liquid: a quantum chemical calculation analysis. *Comput. Theo. Chem.* 1140, 38–48. doi: 10.1016/j.comptc.2018.07.017
- Sha, M., Liu, Y., Dong, H., Luo, F., Jiang, F., Tang, Z., et al. (2016). Origin of heterogeneous dynamics in local molecular structures of ionic liquids. *Soft Matt.* 12, 8942–8949. doi: 10.1039/C6SM01797E
- Shah, F. U., Glavatskih, S., and Antzutkin, O. N. (2013). Boron in tribology: from borates to ionic liquids. *Tribol. Lett.* 51, 281–301. doi: 10.1007/s11249-013-0181-3
- Shah, F. U., Glavatskih, S., MacFarlane, D. R., Somers, A., Forsyth, M., and Antzutkin, O. N. (2011). Novel halogen-free chelated orthoborate-phosphonium ionic liquids: synthesis and tribophysical properties. *Phys. Chem. Chem. Phys.* 13, 12865–12873. doi: 10.1039/c1cp21139k
- Shah, F. U., Holmgren, A., Rutland, M. W., Glavatskih, S., and Antzutkin, O. N. (2018). Interfacial behavior of orthoborate ionic liquids at inorganic oxide surfaces probed by nmr, ir, and raman spectroscopy. *J. Phys. Chem. C* 122, 19687–19698. doi: 10.1021/acs.jpcc.8b06049
- Taher, M., Shah, F. U., Filippov, A., De Baets, P., Glavatskih, S., and Antzutkin, O. N. (2014). Halogen-free pyrrolidinium bis (mandelato) borate ionic liquids: some physicochemical properties and lubrication performance as additives to polyethylene glycol. *RSC Adv.* 4, 30617–30623. doi: 10.1039/C4RA02551B
- Wang, H., Gurau, G., and Rogers, R. D. (2012). Ionic liquid processing of cellulose. *Chem. Soc. Rev.* 41, 1519–1537. doi: 10.1039/c2cs15311d
- Wang, Y.-L. (2018). Competitive microstructures versus cooperative dynamics of hydrogen bonding and  $\pi$ -type stacking interactions in imidazolium bis (oxalato) borate ionic liquids. *J. Phys. Chem. B* 122, 6570–6585. doi: 10.1021/acs.jpcc.8b02899
- Wang, Y.-L., Laaksonen, A., and Fayer, M. D. (2017a). Hydrogen bonding versus  $\pi$ - $\pi$  stacking interactions in imidazolium-oxalato-borate ionic liquid. *J. Phys. Chem. B* 121, 7173–7179. doi: 10.1021/acs.jpcc.7b05564
- Wang, Y.-L., Li, B., Sarman, S., and Laaksonen, A. (2017b). Microstructures and dynamics of tetraalkylphosphonium chloride ionic liquids. *J. Chem. Phys.* 147:224502. doi: 10.1063/1.4995003
- Wang, Y.-L., Sarman, S., Glavatskih, S., Antzutkin, O. N., Rutland, M. W., and Laaksonen, A. (2015a). Atomistic insight into tetraalkylphosphonium-bis(oxalato) borate ionic liquid/water mixtures. I. Local microscopic structure. *J. Phys. Chem. B* 119, 5251–5264. doi: 10.1021/acs.jpcc.5b00667
- Wang, Y.-L., Sarman, S., Kloos, L., Antzutkin, O. N., Glavatskih, S., and Laaksonen, A. (2016). Solvation structures of water in trihexyltetradecylphosphonium-orthoborate ionic liquids. *J. Chem. Phys.* 145:064507. doi: 10.1063/1.4960506
- Wang, Y.-L., Sarman, S., Li, B., and Laaksonen, A. (2015b). Multiscale modeling of the trihexyltetradecylphosphonium chloride ionic liquid. *Phys. Chem. Chem. Phys.* 17, 22125–22135. doi: 10.1039/C5CP02586A
- Wang, Y.-L., Shah, F. U., Glavatskih, S., Antzutkin, O. N., and Laaksonen, A. (2014). Atomistic insight into orthoborate-based ionic liquids: force field development and evaluation. *J. Phys. Chem. B* 118, 8711–8723. doi: 10.1021/jp503029d
- Watanabe, M., Thomas, M. L., Zhang, S., Ueno, K., Yasuda, T., and Dokko, K. (2017). Application of ionic liquids to energy storage and conversion materials and devices. *Chem. Rev.* 117, 7190–7239. doi: 10.1021/acs.chemrev.6b00504
- Weyman, A., Bier, M., Holm, C., and Smiatek, J. (2018). Microphase separation and the formation of ion conductivity channels in poly (ionic liquid) s:

- a coarse-grained molecular dynamics study. *J. Chem. Phys.* 148:193824. doi: 10.1063/1.5016814
- Wong, L. W.-Y., Alex, S.-F., Tam, G. S.-S., Kan, J. W.-H., Sung, H. H.-Y., Sheong, F. K., et al. (2018). Isolation and enantiostability of the b-chiral bis(salicylato) borate anions [br(sal)<sub>2</sub>] and [bs(sal)<sub>2</sub>]. *RSC Adv.* 8, 1451–1460. doi: 10.1039/C7RA11997F
- Wong, L. W.-Y., Kan, J. W.-H., Nguyen, T.-H., Sung, H. H.-Y., Li, D., Au-Yeung, A. S.-F., et al. (2015). Bis(mandelato)borate: an effective, inexpensive spiroborate anion for chiral resolution. *Chem. Commun.* 51, 15760–15763. doi: 10.1039/C5CC04977F
- Wong, L. W.-Y., Kan, J. W.-H., Sung, H. H.-Y., and Williams, I. D. (2017). Chiral bis(mandelato)borate salts for resolution via metathesis crystallization. *Acta Crystallogr. Sect. C Struct. Chem.* 73, 625–631. doi: 10.1107/S2053229617009718
- Wu, B., Shirota, H., Lall-Ramnarine, S., and Castner, E. W. Jr. (2016). Structure of ionic liquids with cationic silicon-substitutions. *J. Chem. Phys.* 145:114501. doi: 10.1063/1.4962257
- Yllö, A., and Zhang, C. (2019). Experimental and molecular dynamics study of the ionic conductivity in aqueous licl electrolytes. *Chem. Phys. Lett.* 729, 6–10. doi: 10.1016/j.cplett.2019.05.004
- Yu, S., Lindeman, S., and Tran, C. D. (2008). Chiral ionic liquids: synthesis, properties, and enantiomeric recognition. *J. Org. Chem.* 73, 2576–2591. doi: 10.1021/jo702368t
- Zhang, Z., Song, J., and Han, B. (2016). Catalytic transformation of lignocellulose into chemicals and fuel products in ionic liquids. *Chem. Rev.* 117, 6834–6880. doi: 10.1021/acs.chemrev.6b00457
- Zhou, F., Liang, Y., and Liu, W. (2009). Ionic liquid lubricants: designed chemistry for engineering applications. *Chem. Soc. Rev.* 38, 2590–2599. doi: 10.1039/b817899m
- Conflict of Interest:** The authors declare that the research was conducted in the absence of any commercial or financial relationships that could be construed as a potential conflict of interest.
- Copyright © 2020 Pei, Li, Laaksonen and Wang. This is an open-access article distributed under the terms of the Creative Commons Attribution License (CC BY). The use, distribution or reproduction in other forums is permitted, provided the original author(s) and the copyright owner(s) are credited and that the original publication in this journal is cited, in accordance with accepted academic practice. No use, distribution or reproduction is permitted which does not comply with these terms.